Estimation of On-Fly Phase Resistance of on 8/6 Switched Reluctance Motor for Sensorless Control

R. Hrbac[1], T. Mlcak[1], V. Kolar[1], J. Necas[2]
[1]*Department of Electrical Engineering, VSB – Technical University of Ostrava, 17. listopadu 15, 708 33, Czech Republic*
[2]*Institute of Transport, VSB – Technical University of Ostrava, 17. listopadu 15, 708 33, Czech Republic*
roman.hrbac@vsb.cz

***Abstract*—Given that most sensorless methods use the "flux linkage" algorithm for their control, this paper deals with possibilities to improve this sensorless method. When using the sensorless "flux linkage" method it is necessary to know not only the values of phase voltages and currents, but also the correct value of the phase resistance. During the operation of the switched reluctance motor, the value of the phase resistance is significantly changing due to the temperature dependence. Such resistance error causes an inaccurate estimation of the flux linkage. For this reason, it was desirable to implement a sensorless control algorithm for estimating phase resistance. In this paper, the experimental results of the implemented algorithm for estimating the phase resistance under the sensorless operation of a switched reluctance motor are presented. The practical implementation of control of the switched reluctance motor is carried out using a control system with a 16-bit digital signal processor.**

***Index Terms*—Switched Reluctance motors, sensorless control, resistance estimation.**

I. INTRODUCTION

The switched reluctance motor (SRM) is topologically and electromagnetically similar to stepper electric motors with variable reluctance. The main differences of these two motors lie in the design proposal, control methods, as well as performance and application properties. The switched reluctance motor is typically controlled by feedback from the position of the shaft so as to synchronize the commutation of phase currents with the position of the rotor, while the stepper electric motor usually operates in an open-loop, i.e. without any feedback from the position of the shaft. While SRMs are designed for high power conversion efficiency at high speeds, stepper electric motors are designed for greater torque motors with limited speed range. Basic differences are in the geometry of the motor, power electronics and control [1].

II. OPERATION PRINCIPLES OF SRM

The switched reluctance motor is an electric machine. Movement of the SRM may be either rotating or sliding and design of the rotor part internal or external. The stator winding consists of coils wound on each stator pole that are electrically isolated from each other, and can be supplied separately or together. The rotor is made of steel plates. SRM has a number of suitable combinations of stator and rotor poles, while the number of poles on the stator and rotor is always different and in general, there is valid relationship between $N_r = N_s - (N_s / m)$ where m is the number of phases. There is a number of N_s / N_r combinations.

Figure 1 shows one of the most widely used four-phase motors (m = 4) in the configuration of 8/6, which has 24 cycles per revolution and a torque pulse angle of 15°. Winding of each of the two opposite stator poles are connected in series so that their fluxes add and generate a S-J pole pair – the phase.

A pair of coils marked A-A´, B-B´, C-C´ and D-D´ represent one phase. Figure 1 shows that each SRM phase requires one power switching circuit. In the case of switching the power transistors T_1 and T_2 DC voltage is connected to the winding of the relevant SRM phase, and the current starts flowing through the circuit. If the power switches open, the current starts to flow through the zero diodes D_1 and D_2, the voltage on the winding changes its polarity and the current drops down to zero [1], [2].

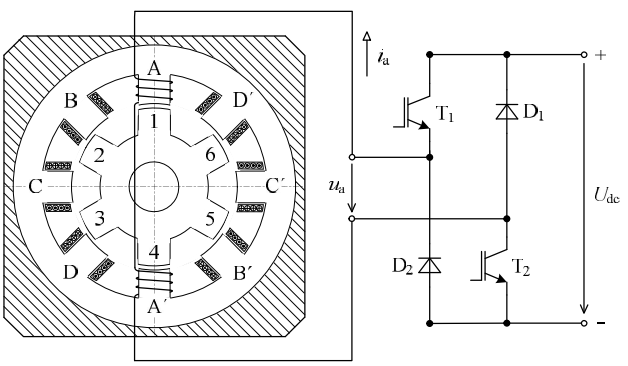

Fig. 1. Four-phase 8/6 SRM with a switched circuit for one phase.

Magnetization characteristics of the SRM define the relationship between the flux linkage and the current for any rotor position. To measure the magnetization characteristics,

Manuscript received October 15, 2013; accepted January 8, 2014.
This research was supported by the project "SP2014/45", by institution of VSB-TU Ostrava.

direct integration method based on (1) below is used

$$\cdot_{\mathrm{j}} = \int (u_{\mathrm{j}} - R_{\mathrm{j}} \times i_{\mathrm{j}})\,\mathrm{d}t, \tag{1}$$

where u_{j} is phase voltage, i_{j} is phase current are measured with a digital oscilloscope. Ψ_{j} is phase flux linkage. An asymmetric bridge of one phase of an inverter, which enables switching ($+U_{\mathrm{dc}}/-U_{\mathrm{dc}}$) and thus a steeper decrease in current, is used for a power circuit.

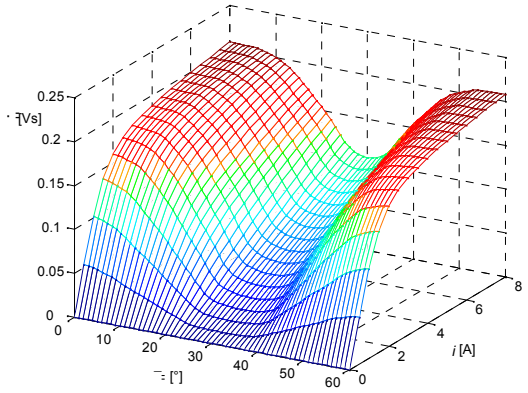

Fig. 2. Magnetization characteristics of SRM ψ (i, θ) approximated by cubic spline.

Measurements were carried out for only one connected phase at the time so as to minimize the effect of other phases, of which winding has been disconnected. From the measured characteristics of flux linkage, the matrix ψ (i, θ) was generated, where the rows of the matrix represent individual positions and the columns of the matrix represent selected values of the currents. A current value of the flux linkage for a given position ¯ and the current i are obtained by quadratic interpolation in the direction i, and by linear interpolation in the direction ¯. Figure 2 shows a three-dimensional graph of the measured magnetization SRM characteristics ψ (i, θ), approximated by cubic spline [3], [4].

III. SENSORLESS CONTROL OF SRM

In the past few years, a number of interesting sensorless methods were designed for the switched reluctance motor [5]–[8]. Despite great advances made in the sensorless control strategy of SRM, none of the current proposals was able to fully replace the mechanical position sensor without this resulting in different limitations in the control of SRM.

The fundamental principle of most sensorless methods is based on the assumption that information about the rotor position can be obtained from measurements of the stator circuit variables or their derived parameters. In other words, information about the position is in fact obtained from the magnetization characteristics of the machine.

When applying the sensorless method based on the evaluation of flux linkage, an incorrectly determined resistance of stator winding affects the accuracy of the estimation of rotor position. The motor operation results in the heating of the stator winding, and thus in the change of its resistance value. The change in stator winding resistance can reach up to 30 % of its nominal value [9]–[12].

A. Estimation of stator winding resistance in SRM

Estimation of stator winding resistance is based on calculation of the flux linkage, which is also used to determine the rotor position. If we neglect the mutual effects of the individual phases, and the current i_{j} of a given phase is equal to zero, then the flux linkage ψ_{j} must also be equal to zero. If this condition has not been met, the (1) evidently shows that the main parameter affecting the flux linkage calculation is the value of winding resistance. Calculation of the flux linkage at the time of current conduction through the given phase is described by the (2) as follows

$$\cdot_{\mathrm{jEstim}} = \int_{t_{\mathrm{on}}}^{t} \left(u_{\mathrm{j}} - R_{\mathrm{jAssume}} \times i_{\mathrm{j}}\right) \mathrm{d}t, \tag{2}$$

where u_{j} and i_{j} are the phase currents and voltages, R_{jAssume} is the assumed value of the phase resistance of the stator winding, and t_{on} is the moment of the voltage conduction into the measured phase of SRM.

Estimated value of the phase winding resistance is defined as the sum of the current value of the phase resistance R_{j} and its variation R_{jError}, as described in (3). Variation of the phase resistance can be caused, for example by a measurement error, an incorrectly defined initial value of the phase resistance or its change in the SRM operation caused by a temperature influence

$$\cdot_{\mathrm{jEstim}} = \int_{t_{\mathrm{on}}}^{t} \left(u_{\mathrm{j}} - (R_{\mathrm{j}} + R_{\mathrm{jError}}) \times i_{\mathrm{j}}\right) \mathrm{d}t = \cdot_{\mathrm{j}} + \cdot_{\mathrm{jError}}. \tag{3}$$

Figure 4 shows the courses of flux linkage for different values of variation of phase resistance during one work cycle of SRM. At the beginning of the work cycle in time t_{on}, DC-Bus voltage is conducted to the given phase, and phase current increases from zero. At the moment of commutation t_{c} the phase stops being supplied with power and current drops down to zero. Similarly, this can be applied to flux linkage, which increases from zero in the $\langle t_{\mathrm{on}}, t_{\mathrm{c}}\rangle$ interval, and from the moment t_{c} it begins to decline until time t_{off}, in which the phase current ceases to exist. If all parameters of (2) are correctly specified and variation of phase resistance R_{Error} is equal to zero, then the composite magnetic flux in time t_{off} must be equal to zero. The described situation is indicated by the course of the flux linkage ψ_{2Estim} in Fig. 3.

The algorithm for estimating the phase resistance is based on the fact that when the phase current is equal to zero, then the flux linkage must be equal to zero at time t_{off}. Under this assumption, it is possible to express the relationship for flux variation in time t_{off} from the (3) follows

$$\cdot_{\mathrm{jEstim}}(t_{\mathrm{off}}) = \cdot_{\mathrm{jError}}(t_{\mathrm{off}}) = -\int_{t_{\mathrm{on}}}^{t_{\mathrm{off}}} (R_{\mathrm{jError}} \times i_{\mathrm{j}})\,\mathrm{d}t. \tag{4}$$

To simplify the process, we further assume that the rate of change of phase resistance during one working cycle SRM is very small. Then the variation of the phase resistance can be written in the form of (5)

$$R_{\mathrm{jError}}(t_{\mathrm{off}}) = \cdot_{\mathrm{jError}}(t_{\mathrm{off}}) / \int_{t_{\mathrm{on}}}^{t_{\mathrm{off}}} i_{\mathrm{j}}\,\mathrm{d}t =$$

$$= \int_{t_{on}}^{t_{off}} \left(u_j - R_{jAssume} \text{ x } i_j \right) dt \,/\, \int_{t_{on}}^{t_{off}} i_j dt. \quad (5)$$

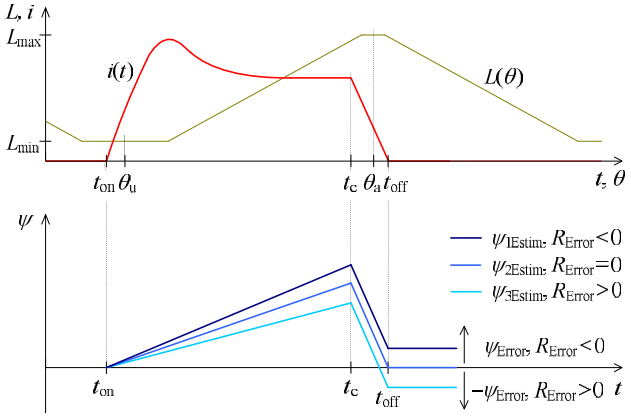

Fig. 3. Effect of the value of phase winding resistance on the course of flux linkage.

In this implementation of sensorless control, flux linkage calculation is performed in each switching period through numerical integration using the trapezoidal method. The same method is used to calculate variation of flux linkage and integral of the phase current, by which the variation of phase stator winding resistance is determined [13], [14].

IV. Estimation of Rotor Position of SRM

With the use of spline functions in the Matlab software, magnetization characteristics were modified so that they can be applied in the algorithm of SRM sensorless control. The m-file that generates the table of magnetization curves was created in Matlab. Each table defines the relationship between rotor position and flux linkage for a given current value. Adjusted magnetization curves for the accurately specified value are shown in Fig. 4. Their number agrees with the number of the tables, which were stored in an external programme memory located on the board MSK2407, which also includes a digital signal processor TMS320LF2407. Blue colour is used for indicating an appropriate area of magnetization characteristics to evaluate the rotor position, and is further divided into three well-defined sectors according to the current strength. This method maximized the accuracy of the evaluation of the rotor position [15]–[18].

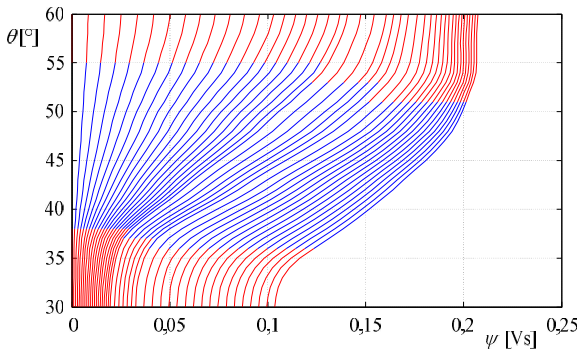

Fig. 4. Table of magnetization characteristics stored in the programme memory, $\theta = f(\psi, i) \mid i = \text{const}$.

Figure 5 shows a block diagram of the applied sensorless control algorithm designed to estimate the rotor position. The measured values of the phase currents and calculated values of flux linkage are entered into the block entitled "Table of measured magnetization curves". To simplify, the calculation of flux linkage of each phase is given by (2).

The output values of the block represent the values of the current rotor position related to different phases, and are determined from the magnetization curves using linear interpolation. Interpolation of the position is performed only in the active SRM phases. In the block entitled "Selection of a suitable phase", the phase from which the rotor position will be evaluated is selected according to the given criteria. Preference is always an active phase, of which the value of an estimated rotor position is located in the appropriate area of evaluation. If there are simultaneously two phases in the appropriate area, or none of them, the phase through which a higher current is conducted is always selected to estimate the rotor position.

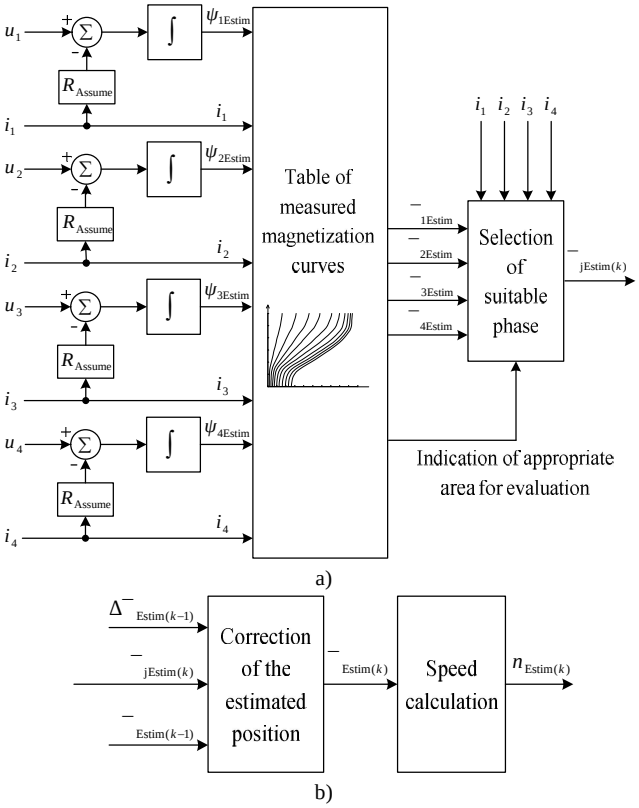

Fig. 5. Simplified block diagram of the algorithm to estimate the rotor position.

In order to eliminate the greater inaccuracies in estimating the rotor position, the block entitled "Correction of the estimated position" has been established. The input variables of this block include: a current estimated rotor position of the selected phase $\theta_{jEstim(k)}$, a value of converted estimated rotor position from the previous switching period $\theta_{Estim(k-1)}$, and change of the estimated position $\theta_{Estim(k-1)}$, which was calculated in the previous switching period from the most suitable phase.

V. Flux Linkage Calculation in the Discrete Domain

During motor operation, the phase current and the phase voltage are measured regularly in rates of the sampling frequency. The flux linkage estimation is based on these measurements. In order to increase the precision of the integration a trapezoidal integration is used. Equation (2)

can be converted to

$$\psi_{j(N)} = \sum_{k=1}^{N} 1/2 \text{ x } [g_{j(k-1)} + g_{j(k)}] \text{ x } T_{PWM}, \quad (6)$$

where T_{PWM} is the sampling period, $g_{j(k)}$ is calculated according to (7) and $\psi_{j(N)}$ is the calculated magnetic flux linkage for the measurement cycle N.

The flux linkage is calculated regularly in each sampling cycle from the beginning of the commutation stroke (t_{on}). The sampling period T_{PWM} is constant. Because the sampling period is kept constant, the division can be considered as a scaling factor

$$g_{j(k)} = d_{1(k)} \text{ x } [U_{dc(k)} - (R_{jAssume} + 2 \text{ x } R_T) \text{ x } i_{j(k)}] + \\ + d_{2(k)} \text{ x}[(-R_{jAssume} - R_T - R_D) \text{ x } i_{j(k)} - u_D + \\ + d_{3(k)} \text{ x } [-U_{dc(k)} - (R_{jAssume} + 2R_D) \text{ x } i_{j(k)} - 2 \text{ x } u_D], \quad (7)$$

where $d_{1(k)}$ is calculated regularly in each sampling cycle from the equation $d_{1(k)} = t_{1(k)}/T_{PWM}$ (t_1 is time when both transistors T1 and T2 are turned-on, as shown in Fig. 1), $d_{2(k)}$ from the equation $d_{2(k)} = t_{2(k)}/T_{PWM}$ (t_2 is time when transistor T1 is turned-off and T2 is turned-on) and $d_{3(k)}$ from the equation $d_{3(k)} = t_{3(k)}/T_{PWM}$ (t_3 is time when both transistors T1 and T2 are turned-off and both diodes conduct the current). $U_{dc(k)}$ and $i_{j(k)}$ is the sampled DC-Bus voltage and the phase current. The phase voltage is not measured directly. The DC-Bus voltage is measured instead and the phase voltage is calculated according to the applied PWM duty cycle.

The integral of the phase current according to (5) can be also expressed as a sum of individual samples over the current pulse

$$I_{j(N)} = \sum_{k=1}^{N} 1/2 \text{ x } [i_{j(k-1)} + i_{j(k)}] \text{ x } T_{PWM}. \quad (8)$$

Then (5) can be expressed as

$$R_{jError} = \sum_{k=1}^{N} 1/2 \text{ x } [g_{j(k-1)} + g_{j(k)}] \text{ x } T_{PWM} / \\ / \sum_{k=1}^{N} 1/2 \text{ x } [i_{j(k-1)} + i_{j(k)}] \text{ x } T_{PWM} = \\ = \sum_{k=1}^{N} [g_{j(k-1)} + g_{j(k)}] / \sum_{k=1}^{N} [i_{j(k-1)} + i_{j(k)}], \quad (9)$$

where N is the last sample taken when the phase current disappears to zero.

The actual phase resistance can be expressed as

$$R_j = R_{Assumed} - \sum_{k=1}^{N} [g_{j(k-1)} + g_{j(k)}] / \\ / \sum_{k=1}^{N} [i_{j(k-1)} + i_{j(k)}], \quad (10)$$

where $R_{Assumed}$ is the assumed phase winding resistance. Equation (10) can be efficiently used for the correct resistance calculation.

VI. Experimental Results of Stator Winding Resistance Estimation Measured on Real SRM Drive

This chapter presents the estimate results of stator winding phase resistance during the SRM operation. An algorithm providing the current value of the phase resistance is, in order to improve the estimate of the rotor position used in a sensorless method, based on the evaluation of the flux linkage.

Control algorithms were tested with the use of MSK2407 development kit equipped with a TMS320LF2407 signal processor. The MSK2407 kit contains an external memory, which was also used to save up to 8 selected variables of the application software (i.e. motor speed, actual and estimated rotor position, flux linkage, etc.). These variables were investigated with the use of DMC Developer Pro software, and then saved as text files and drawn in Microsoft Excel spreadsheet. All graphs presented in this chapter were obtained in this way.

Experimental measurement was carried out on a real drive equipped with a switched reluctance motor SR90. This is a 4-phase 8/6 SRM. Its rated power is P_n = 400 *W*, rated speed n_n = 3000 *rpm* and M_n = 0.3 *Nm*. This SRM was powered by a frequency converter, where DC link voltage U_{dc} = 100 *V* and switching frequency f_{PWM} = 10 *kHz*.

Figure 6 (above) shows the phase current courses and calculated flux linkage with the set reference value of the phase resistance to be 20 % higher than its actual value. The measurements are performed in a stable state n_{Ref} = 300 *rpm* and feedback from the algorithm estimating phase resistance is intentionally not implemented. The course of the flux linkage also shows an influence of the value of the phase resistance on its exact determination. The resistance estimation algorithm is based on the fact that when phase current equals zero, magnetic flux has to equal zero as well. Resistance error leads to the flux estimation error. Since resistance estimation error is positive (+20 %), flux linkage error is negative for time t_{on}, as described in Chapter 3. Figure 6 (below) compares the courses of actual and estimated rotor positions, which is determined from the magnetization characteristics of SRM using measured phase current and calculated flux linkage. Estimated position θ_{Estim} graph makes it possible to observe the effect of incorrectly selected phase resistance value on the estimation of SRM rotor position, using the flux linkage based sensorless method.

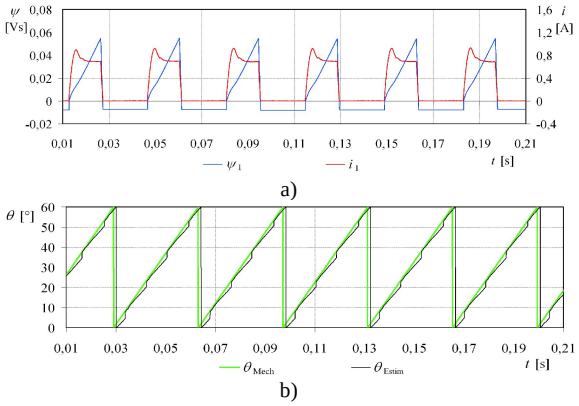

Fig. 6. Effect of winding resistance on calculation of the flux linkage and on the rotor position estimate accuracy when n_{Ref} = 300 *rpm* and R_{Ref} = +20 % without resistance correction.

Figure 7 shows the phase current courses and calculated flux with the set reference value of the phase resistance to be 20 % lower than its actual value and with n_{Ref} = 300 *rpm*. Because the resistance estimation error is negative (-20 %), the flux linkage error is positive for time t_{on}, as described in

Chapter 3.

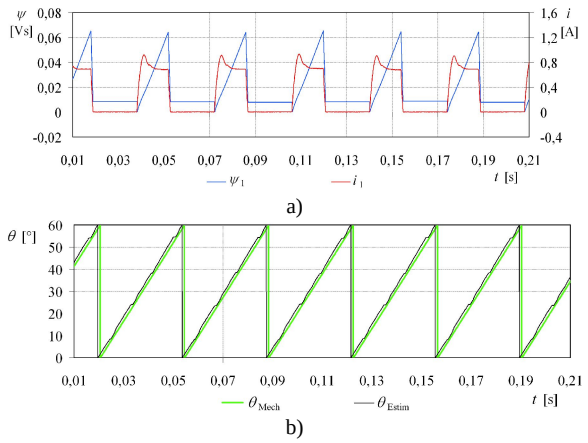

Fig. 7. Effect of winding resistance on calculation of the flux linkage and on the rotor position estimate accuracy when n_{Ref} = 300 *rpm* and R_{Ref} = -20 % without resistance correction.

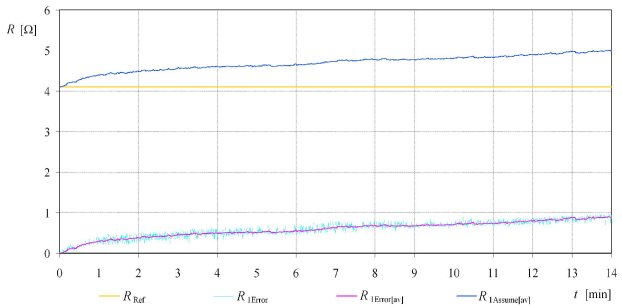

Fig. 8. Estimate of winding resistance during SRM operation when n_{Ref} = 600 *rpm* and a preset load $M_L = M_N$.

Figure 8 shows an estimated winding resistance during the SRM operation over a longer time period and a preset load of working mechanism $M_L = M_N$. The curve courses show an initial value of the phase resistance R_{Ref}, variation of phase resistance R_{1Error}, calculated each business cycle in the phase 1, corrected phase variation $R_{1Error[av]}$, and an estimated value of the phase resistance $R_{1Assume[av]}$. The picture shows that when SRM was loaded with nominal torque, phase resistance increased by 0.9 Ω in 14 minutes, which means an increase by 22 %. This demonstrates very clearly the effect of coil heating during SRM operation on its coil resistance.

Figure 9 to Fig. 12 show the actual position and the estimated position, the estimated rotor position error, the estimation of rotor position of the individual phases and the number of the phase from which the rotor position is evaluated during sensorless control of the SRM at n_{Ref} = 420 *rpm*. The graph in Fig. 10 shows that the variation θ_{Error} fluctuates in a range of ±2°. The principle of determining a suitable phase that is selected to estimate rotor position is described in Chapter 4.

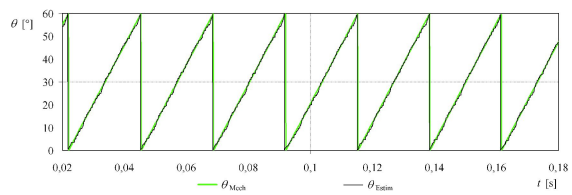

Fig. 9. Actual position and estimated position during sensorless control of the SRM at n_{Ref} = 420 *rpm*.

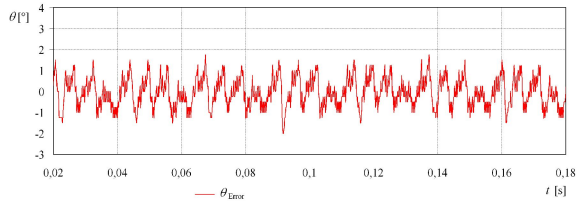

Fig. 10. Estimated rotor position error during sensorless control of the SRM at n_{Ref} = 420 *rpm*.

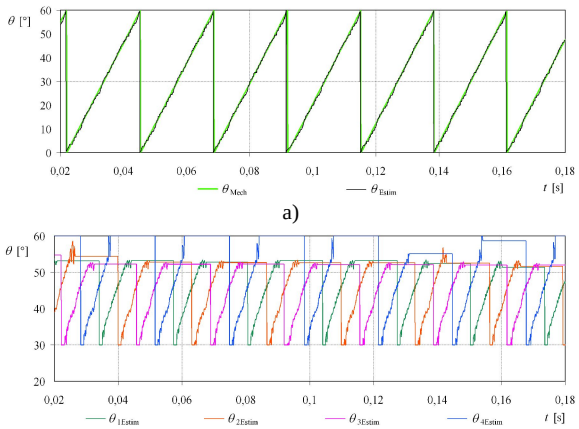

Fig. 11. Estimation of rotor position of the individual phases during sensorless control of the SRM at n_{Ref} = 420 *rpm*.

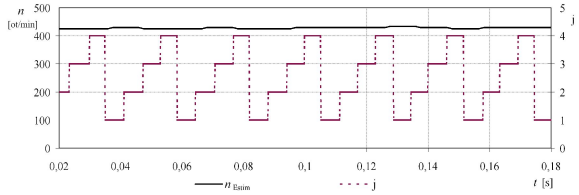

Fig. 12. Number of the phase from which the rotor position is evaluated during sensorless control of the SRM at n_{Ref} = 420 *rpm*.

Figure 13 to Fig. 14 show the actual position and the estimated position, actual phase currents i_2 and i_4 during sensorless control of the SRM motor at n_{Ref} = 250 *rpm*. Figure 14 shows that phase currents i_2 and i_4 are limited, so they do not exceed a maximum 4 *A* value.

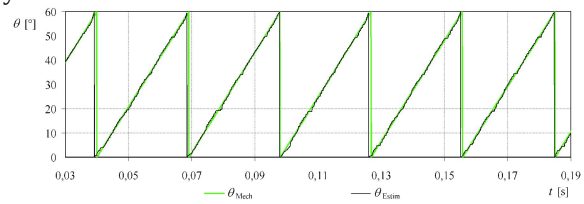

Fig. 13. Actual position and estimated position during sensorless control of the SRM at n_{Ref} = 250 *rpm*.

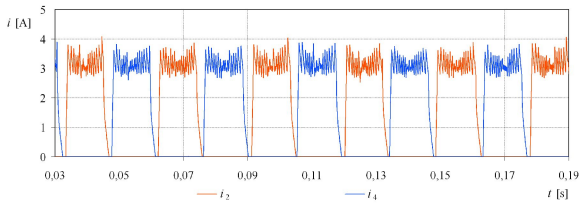

Fig. 14. Actual phase currents i_2 and i_4 during sensorless control of the SRM at n_{Ref} = 250 *rpm*.

Figure 15 to Fig. 18 show the actual position and the estimated position, actual speed and estimated speed, phase current i_2 and flux linkage ψ_2 during sensorless control of the SRM at n_{Ref} = 0 to 1750 *rpm*. Figure 16 shows that

sensorless algorithm controlling the SRM contains a startup routine. First, the rotor rotates in its initial position, determined by Phase A (Fig. 1).

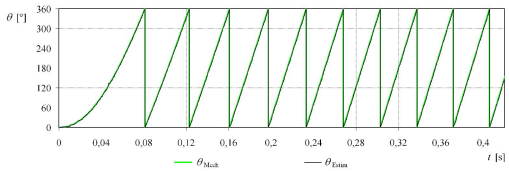

Fig. 15. Actual position and estimated position during sensorless control of the SRM at n_{Ref} = 0 to 1750 *rpm*.

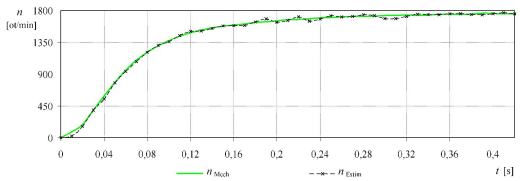

Fig. 16. Actual speed and estimated speed during sensorless control of the SRM at n_{Ref} = 0 to 1750 *rpm*.

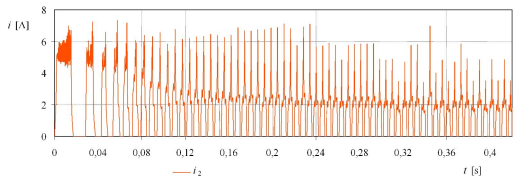

Fig. 17. Actual current i_2 during sensorless control of the SRM at n_{Ref} = 0 to 1750 *rpm*.

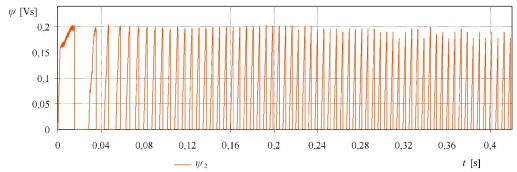

Fig. 18. Actual flux linkage ψ_2 during sensorless control of the SRM at n_{Ref} = 0 to 1750 *rpm*.

The functionality of this applied algorithm determining the phase resistance of SRM stator winding, has been proved by practical results.

VII. CONCLUSIONS

The real 8/6 switched reluctance motor with a power of 400 *W* was used for experimental measurements. For such a low power motor, the price of a position sensor is comparable to the price of the motor. Therefore, efforts were made to design, with the use of microprocessor technology, a control algorithm to control SRM without the position sensor.

The paper deals with the sensorless control of the switched reluctance motor, particularly with the influence and estimation of phase resistance during motor operation. This control only uses the DC-Bus voltage and phase currents to estimate the rotor position, which can be easily measured from the motor connection terminals. The phase resistance estimation algorithm was developed based on the phase flux linkage calculation and its relation to the phase current. Experimental results confirm that without the proper phase resistance estimation, it is very difficult to control the sensorless SR drive according to the optimal motor characteristics linked to the rotor position due to the fact that resistance significantly changes with the temperature of the motor. Using the phase resistance estimation algorithm, the rotor position estimation error at middle and lower speeds is below 2 %. An applied "flux linkage" sensorless method is suitable for the area of middle and higher revolutions per minute, where there are no inaccuracies in the calculation of the flux linkage caused by a large number of integration steps.

REFERENCES

[1] T. J. E. Miller, *Electronic Control of Switched Reluctance Machines*. Newnes, 2001.

[2] M. Alrifai, M. Zribi, M. Rayan, "Speed control of switched reluctance motors taking into account mutual inductances and magnetic saturation effects", *Energy Conversion and Management*, vol. 51, no. 6, pp. 1287–1297, 2010.

[3] A. Kakilli, "Magnetic analysis of modified-rotor switched reluctance motor", *Elektronika Ir Elektrotechnika*, no. 9, pp. 21–26, 2011. Online [Available]: http://dx.doi.org/10.5755/j01.eee.115.9.742

[4] R. Dolecek, O. Cerny, J. Novak, M. Bartlomiejczyk, "Interference in power system for traction drive with PMSM", *Przeglad Elektrotechniczny*, no. 88, vol. 9a, pp. 204–207, 2012.

[5] Yan-Tai Chang, Ka Wai Eric Cheng, "Sensorless position estimation of switched reluctance motor at startup using quadratic polynomial regression", *IET Electric Power Applications*, vol. 7, no. 7, pp. 618–626. Online [Available]: http://dx.doi.org/10.1049/iet-epa.2012.0306, 2013

[6] J. Cai, Z. Deng, "A position sensorless control of switched reluctance motors based on phase inductance slope", *Journal Of Power Electronics*, vol. 13, no. 2, pp. 264–274.

[7] R. X. Antoni, M. Hilairet, "Enhancing the flux estimation based sensorless speed control for switched reluctance machines", *Electric Power Systems Research*, vol. 104, pp. 62–70, 2013.

[8] R. Zhong, Y. B. Wang, Y. Z. Xu, "Position sensorless control of switched reluctance motors based on improved neural network", *IET Electric Power Applications*, vol. 6, no. 2, pp. 111–121.

[9] A. Loria, G. Espinosa-Perez, E. Chumacero, "Speed-sensorless control of switched-reluctance motors with uncertain payload", *American Control Conf.*, Washington, DC, 2013, pp. 3437–3442.

[10] A. Arias, X. Rain, M. Hilairet, "Enhancing the flux estimation based sensorless speed control for switched reluctance machines", *Electric Power Systems Research*, vol. 104, pp. 62–70, 2013.

[11] Ming-Yen Wei, Tian-Hua Liu, "A high-performance sensorless position control system of a synchronous reluctance motor using dual current-slope estimating technique", *IEEE Trans. Industrial Electronics*, vol. 59, no. 9, pp. 3411–3426, 2012.

[12] P. Brandstetter, T. Krecek, "Sensorless control of permanent magnet synchronous motor using voltage signal injection", *Elektronika ir Elektrotechnika*, vol. 19, no. 6, pp. 19–24, 2013. Online [Available]: http://dx.doi.org/10.5755/j01.eee.19.6.1583

[13] B. Karanayil, M. F. Rahman, C. Grantham, "Online stator and rotor resistance estimation scheme using artificial neural networks for vector controlled speed sensorless induction motor drive", *IEEE Trans. Industrial Electronics*, vol. 54, no. 1, pp. 167–176, 2007. Online [Available]: http://dx.doi.org/10.1109/TIE.2006.888778

[14] R. Visinka, "Phase resistance estimation for sensorless control of switched reluctance motors", in *Proc. 28th Annual Conf. IEEE Industrial-Electronics-Society*, Univ Sevilla, Spain, 2002, pp. 1044–1049.

[15] H. Moradi, E. Afjei, "Novel rotor position estimation technique for switched reluctance motor (SRM)", *International Journal of Electronics*, vol. 98, no. 9, pp. 1169–1184, 2011.

[16] J. Uma, A. Jeevanandham, "Sensorless control in switched reluctance motor drives for four quadrant operation" *IEEE Int. Multi Conf. Automation, Computing, Communication, Control and Compressed Sensing (Imac4s)*, India, 2013, pp. 420–424.

[17] S. Kocman, P. Orsag, P. Svoboda, "Influence of supply voltage quality on harmonics generated by AC adjustable speed drives", *Przeglad elektrotechniczny*, vol. 88, no. 10a, pp. 302–304, 2012.

[18] P. Kacor, "Axial generator for small wind power plant", in *Proc. 13th Int. Scientific Conf. Electric Power Engineering*, VUT Brno, Czech Republic, 2012, pp. 1149–1153.